Femtosecond laser point-by-point inscription of an ultra-weak fiber Bragg grating array for distributed high-temperature sensing

BAIJIE XU,[1,2] **JUN HE,**[1,2,*] **BIN DU,**[1,2] **XUNZHOU XIAO,**[1,2] **XIZHEN XU,**[1,2] **CAILING FU,**[1,2] **JIA HE,**[1,2] **CHANGRUI LIAO,**[1,2] **AND YIPING WANG**[1,2]

[1]*Key Laboratory of Optoelectronic Devices and Systems of Ministry of Education/Guangdong Province, College of Physics and Optoelectronic Engineering, Shenzhen University, Shenzhen 518060, China*
[2]*Shenzhen Key Laboratory of Photonic Devices and Sensing Systems for Internet of Things, Guangdong and Hong Kong Joint Research Centre for Optical Fibre Sensors, Shenzhen University, Shenzhen 518060, China*
*hejun07@szu.edu.cn

Abstract: Ultra-weak fiber Bragg grating (UWFBG) arrays are key elements for constructing large-scale quasi-distributed sensing networks for structural health monitoring. Conventional methods for creating UWFBG arrays are based on in-line UV exposure during fiber drawing. However, the UV-induced UWFBG arrays cannot withstand a high temperature above 450 °C. Here, we report for the first time, to the best of our knowledge, a new method for fabricating high-temperature-resistant UWFBG arrays by using a femtosecond laser point-by-point (PbP) technology. UWFBGs with a low peak reflectivity of ∼ - 45 dB (corresponding to ∼ 0.0032%) were successfully fabricated in a conventional single-mode fiber (SMF) by femtosecond laser PbP inscription through fiber coating. Moreover, the influences of grating length, laser pulse energy, and grating order on the UWFBGs were studied, and a grating length of 1 mm, a pulse energy of 29.2 nJ, and a grating order of 120 were used for fabricating the UWFBGs. And then, a long-term high-temperature annealing was carried out, and the results show that the UWFBGs can withstand a high temperature of 1000 °C and have an excellent thermal repeatability with a sensitivity of 18.2 pm/°C at 1000 °C. A UWFBG array consisting of 200 identical UWFBGs was successfully fabricated along a 2 m-long conventional SMF with an interval of 10 mm, and interrogated with an optical frequency domain reflectometer (OFDR). Distributed high-temperature sensing up to 1000 °C was demonstrated by using the fabricated UWFBG array and OFDR demodulation. As such, the proposed femtosecond laser-inscribed UWFBG array is promising for distributed high-temperature sensing in hash environments, such as aerospace vehicles, nuclear plants, and smelting furnaces.

1. Introduction

Distributed temperature sensing (DTS) at high temperatures ranging from 400 °C to above 1000 °C are required in many areas, such as aerospace vehicles, oil and gas explorations, blast furnaces, and power stations. To date, various DTS methods have been achieved by using the intrinsic scattering effects (i.e. Raman [1–3], Brillouin [1,4,5], and Rayleigh [1,6,7]) in optical fibers. Temperature information can be recovered from the intensity changes or frequency shifts in the backscattered signals. Conventional Raman- or Brillouin-based DTS methods are suitable for measuring the temperature in a long sensing range (more than tens of kilometers) with a low spatial resolution (on the order of 1 meter) [2–5]. A Rayleigh-based DTS with optical frequency domain reflectometer (OFDR) demodulation has a higher spatial resolution (on the order of millimeters) but a limited sensing range (up to several tens of meters) [6,7]. Moreover, DTS at a high temperature of above 800 °C has also been achieved by using these techniques with specialty

fibers, such as gold-coated fiber [8,9], pure silica photonic crystal fiber (PCF) [10], and single crystal fiber [11,12]. However, these methods typically have low signal-to-noise-ratio (SNR) due to the extremely weak intrinsic backscattering in optical fiber and hence require more time for signal processing [1]. In contrast, the reflective intensity of an ultra-weak fiber Bragg grating (UWFBG) is several orders of magnitude higher than that of intrinsic backscattering [13,14]. The UWFBG can provide a much higher SNR, and hence ensures a fast and accurate wavelength demodulation for DTS [13–15].

To date, various methods have been developed for mass production of UWFBGs by using UV exposure [16,17]. For example, the researchers at Virginia Polytechnic Institute and State University established an automated UWFBG fabrication system by using a UV phase-mask exposure method, and successfully fabricated an UWFBG array consisting of 1000 identical UWFBGs with a very low reflectivity of ∼ - 40 dB [18]. Note that a CO_2 laser-based coating pre-removal process and a recoating process are required before and after UV exposure. This additional coating and recoating process will degrade the mechanical strength of the UWFBG. In addition, the in-line approaches are reported for inscribing a large number of UWFBGs during the fiber drawing process by using UV exposure with a Talbot interferometer [19–21] or a phase mask [22–25]. For example, in 1993, Dong *et al.* reported the fabrication of draw tower gratings (DTGs) by using a Talbot interferometer for the first time [19]. Moreover, the researchers at Wuhan University of Technology have fabricated 10,000 DTGs along a 10 m-long fiber by using a UV phase-mask method during fiber drawing [25]. The results show that these in-line methods can be used for producing DTGs at a very high speed and the produced UWFBGs have high mechanical strength, and hence these DTGs are suitable for large-scale multiplexing. Unfortunately, these UV-induced DTGs are type I gratings and can operate at a low temperature of below 450 °C [26,27]. As a result, efforts have been made to improve the thermal stability of the fabricated DTGs. For example, the researchers at Institute of Photonic Technology (IPHT) fabricated type II DTGs by using higher laser pulse energy and exhibited a high operation temperature of up to 900 °C [20]. However, the reflectivity in such a type II DTG is too high, and these DTGs typically have poor spectral quality and large insertion loss. Later, they reported the fabrication of thermally regenerated DTGs, which could be used at a high temperature of 800 °C [21]. In addition, the researchers at University of Mons reported a thermally regenerated FBG, which can withstand a higher temperature of 900 °C [28]. However, additional hydrogen loading and thermal regeneration process are required for fabricating such a thermally regenerated DTG.

Femtosecond laser, featuring by ultra-short pulse width and extremely high peak intensity, is a powerful tool for fabricating various FBGs that can operate at high temperatures [29–36]. Type II FBGs with structural changes can be inscribed by using high-intensity femtosecond lasers and can withstand a high temperature of above 1000 °C [33,34]. Moreover, FBGs with improved temperature resistance were fabricated in pure-silica photonic crystal fibers (PCFs) [35] and single-crystal sapphire optical fibers [36]. Nevertheless, it should be noted that these femtosecond laser-induced FBGs have a high reflectivity, which is detrimental to large-scale multiplexing and cannot be used for distributed high-temperature sensing. To date, there are few reports on the fabrication of UWFBGs by using a femtosecond laser.

In this work, we report for the first time, to the best of our knowledge, a new method for fabricating UWFBGs based on a femtosecond laser PbP technology. UWFBGs with a peak reflectivity of ∼ - 45 dB were successfully fabricated by using grating length of 1 mm, laser pulse energy of 29.2 nJ, and grating order of 120. The fabricated UWFBGs can withstand a very high temperature of 1000 °C for 35 hours and exhibit an excellent thermal repeatability. Subsequently, an UWFBG array consisting of 200 identical UWFBGs was constructed along a 2 m-long single-mode fiber (SMF) with an interval of 10 mm, and then interrogated with a commercial OFDR. Moreover, the fabricated UWFBG array was demonstrated for distributed

high-temperature sensing up to 1000 °C with OFDR demodulation. Such a femtosecond laser-induced identical UWFBG array could further be developed for distributed high-temperature sensing under extreme conditions.

## 2. Experimental setup for fabricating and interrogating UWFBG arrays

2.1. Experimental setup for fabricating UWFBG arrays

Figure 1 illustrates the experimental setup for fabricating UWFBG arrays with a femtosecond laser PbP technology. We employed a frequency-doubled regenerative amplified Yb:KGW (KGd(WO$_3$)) femtosecond laser (Pharos, Light-Conversion) with a wavelength of 514 nm, a pulse width of 290 fs, and a repetition rate of 200 kHz as the laser source. A waveplate and Glan polarizer were used to adjust the optical power and polarization of the laser beam. A dichroic mirror was used for reflecting the laser beam to the objective and transmitting the visible illumination beam to the CCD. A Leica oil-immersion objective (100×, NA=1.25) was adopted for focusing the laser beam onto the fiber core center, and the reflective index oil ($n \approx$ 1.4587) was applied on the space between fiber and objective, and the aberration induced by the cylindrical fiber geometry could be minimized. A conventional SMF (Corning SMF-28) with polymer coating was fixed by a pair of fiber holders mounted on a 3D high-precision air-bearing translation stage (assembled by Aerotech ABL15010, ANT130LZS, and ANT130V-5). Note that no pre-removal of fiber coatings was required before grating inscription. Moreover, a fiber feeding system consisting of pulley, stepper motor, and fiber spool was established for automatically translating the fiber to a preset position. During the UWFBG inscription process, the laser beam was fixed and the optical fiber was moved by the translation stage, and the top-view microscope images of fiber core was captured by the CCD for real-time positioning the fiber core center. An image recognition algorithm was used in the femtosecond PbP technology for auto-aligning the laser beam focus within the fiber core center. Hence, the automatic fabrication of UWFBGs could be achieved by simultaneously controlling the shutter, fiber holders, translation stages, step motor, and CCD with a personal computer (PC). Moreover, a commercial OFDR (LUNA, OBR 4600) was used to monitor the wavelength of each UWFBG at different positions in the array.
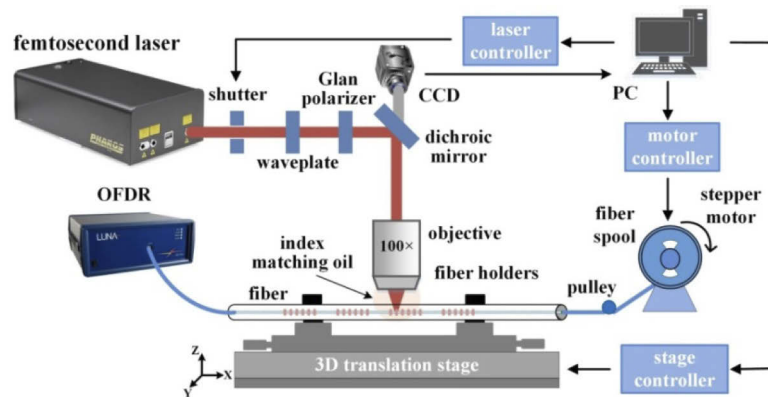
Fig. 1. Experimental setup for fabricating UWFBG array by using a femtosecond laser PbP technology.

The process for fabricating a UWFBG array involves five main steps. In step 1, a section of SMF with coating layer was fixed with a pair of fiber holders on the 3D translation stage. One end of the SMF was connected to the OFDR, and the other end of SMF was winded onto a fiber spool. The axial direction of SMF was adjusted parallel to the x-axis of the translation stage. In step 2, the SMF was precisely translated along the y- and z-axes to ensure the laser
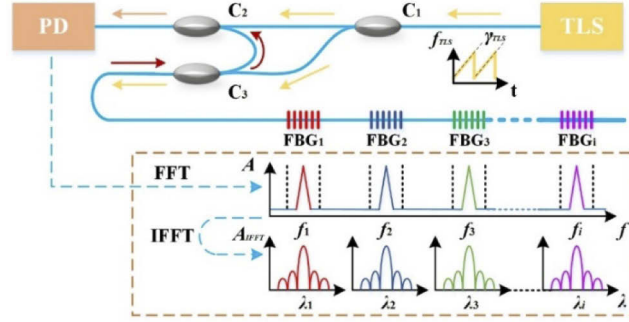
Fig. 2. Schematic of simplified experimental setup and demodulation process of an OFDR-based wavelength demodulation for UWFBG array.

beam focus could be aligned with the fiber core center. Note that this step was implemented in assistance with an image recognition technique, in which the fiber core center was recognized by finding the core/cladding boundaries from the top-view microscope images via a Gaussian smoothing algorithm and subsequent gray-scale intensity profile extracting algorithm. In step 3, the shutter was opened and the femtosecond laser beam was focused onto the fiber core center through the fiber coating. In this step, the SMF was translated along the x-axis at a constant speed, and a series of index modulation points were created along the fiber axis, i.e. a UWFBG was fabricated in the fiber core. Subsequently, in step 4, the fiber holders were loosed, and the SMF was translated to a preset position along the fiber by rotating the fiber spool via a step motor in the fiber feeding system. Then, in step 5, the two fiber holders were closed again, and the second UWFBG was fabricated by repeating the step 2 and step 3. Moreover, the third to the Nth UWFBG could be fabricated by executing the same process (i.e., by repeating the step 4 and step 5). As a result, a UWFBG array was successfully fabricated by using the femtosecond laser PbP technology. Moreover, it should be noted that the opening and closing of the fiber holders and shutters, the movements of 3D translation stage and step motor, and the image acquisition by CCD were all controlled automatically by PC. As a result, an efficient fabrication of the identical UWFBG array has been achieved.

2.2. OFDR-based wavelength demodulation for identical UWFBG array

The OFDR technique was used for interrogating the Bragg wavelength of each UWFBG at different locations in the fabricated identical UWFBG array. The principle of OFDR-based UWFBG wavelength demodulation is illustrated in Fig. 2. The system can be simplified into a Mach-Zehnder interferometer, i.e., the output of a tunable laser source (TLS) is split into two paths by a fiber coupler and the test UWFBG array is placed in one path of the interferometer. In case the optical frequency of the TLS f_{TLS} is swept at a constant speed of γ_{TLS}, the optical interference signal illuminated on the photodetector (PD) is given by [6,37]

$$
\begin{aligned}
I(t) &= \eta I_0 \cdot \sum_{i=1}^{N} \left\{ r_i \cdot \cos\left[2n\Delta L_i \cdot \frac{2\pi f_{TLS}(t)}{c} \right] \right\} = I_M \cdot \sum_{i=1}^{N} \{ r_i \cdot \cos[2\pi \cdot \gamma_{TLS} t \cdot \Delta \tau_i] \} \\
&= I_M \cdot \sum_{i=1}^{N} \{ r_i \cdot \cos[2\pi \cdot \gamma_{TLS} \Delta \tau_i \cdot t] \} = I_M \cdot \sum_{i=1}^{N} \{ r_i \cdot \cos[2\pi f_i t] \},
\end{aligned}
\tag{1}
$$

where I_0 and I_M are the intensity of the incident beam and reference beam, respectively, η is the insertion loss of the interferometer, n is the effective refractive index of the propagation mode, and N is the total number of UWFBGs. $\Delta L_i, \Delta \tau_i, f_i,$ and r_i are the path difference, time

delay, beat frequency, and reflectivity of the ith UWFBG, respectively. As shown in Fig. 2, a fast Fourier transform (FFT) is applied to the interference signal shown in Eq. (1), and the position information of each UWFBG could be resolved through f_i obtained in the frequency domain. Furthermore, a sliding window (i.e., a band-pass filter with appropriate bandwidth) is applied to the selected UWFBG in frequency domain, and an inverse fast Fourier transform (IFFT) is applied. The beat signal at the frequency of the selected UWFBG could be separated from the interference signal and the optical spectrum of a specific UWFBG in the identical UWFBG array could be obtained. Hence, distributed temperature sensing could be achieved by tracking the shift in the peak wavelength of each UWFBG.

3.　Device fabrication and high-temperature annealing of UWFBGs

3.1.　Principle of PbP UWFBGs

The peak reflectivity of an FBG can be expressed as [38]

$$R_{\text{max}} = \tanh^2(\kappa \cdot L), \tag{2}$$

where $\kappa \cdot L$ is the grating strength, L is the grating length, and κ is the coupling coefficient. In a strong FBG (i.e. $R_{\text{max}} > 90\%$), the calculated grating strength of $\kappa \cdot L$ is larger than 2. In contrast, a UWFBG with ultra-weak reflectivity of - 40 dB has a very small $\kappa \cdot L$ of merely 0.01, which is two orders of magnitude lower than that of a strong FBG. Note that a UWFBG with such a low reflectivity is easy for large-scale multiplexing, since the multiple reflection-induced crosstalk and spectral distortion in the FBG array could be reduced significantly [15]. Moreover, it could be seen from Eqs. (2) and (3) that the UWFBG peak reflectivity depends on the grating length L and the coupling coefficient κ. The decrease in grating length L leads to a reduced grating reflectivity but a broadened grating bandwidth [36]. A large bandwidth is disadvantageous to wavelength demodulation. Another approach for reducing the reflectivity is to reduce the coupling coefficient κ, which could be expressed as

$$\kappa = \frac{\pi}{\lambda} \int_{-\infty}^{\infty} \int_{-\infty}^{\infty} \Delta n(x, y) E(x, y) E^*(x, y) dx dy, \tag{3}$$

where $\Delta n(x, y)$ is the localized effective refractive index modulation created by femtosecond laser inscription. It is obvious that the coupling coefficient κ is determined by the refractive index modulation and the overlap between the index modulation area and mode field distribution. Hence, the femtosecond laser PbP technology is an effective way to fabricate UWFBGs since it could produce a very small index modulation point inside the fiber core and leads to a small coupling coefficient κ. In addition, the coupling coefficient κ could be further reduced by decreasing the localized effective refractive index modulation $\Delta n(x, y)$, which could be achieved either by using a femtosecond laser with decreased pulse energy E or by using a higher grating order K. As a result, UWFBGs can be created by using the femtosecond laser PbP technology with appropriate fabrication parameters including the grating length L, pulse energy E, and grating order K.
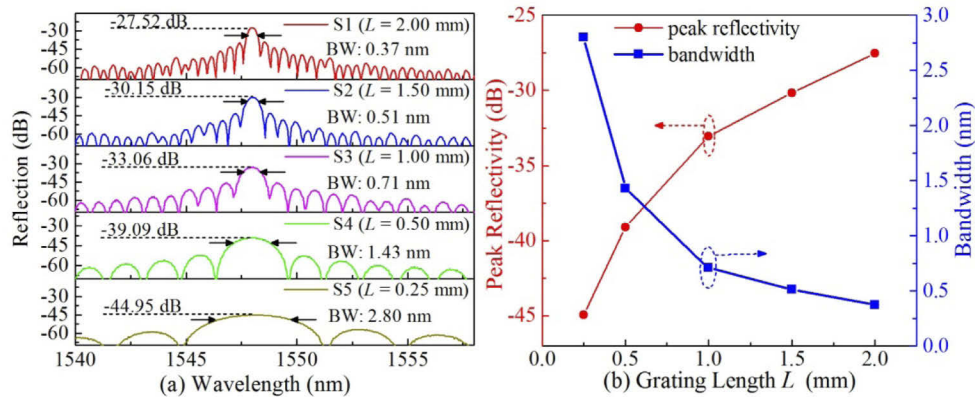
3.2.　Influence of grating length on UWFBG

At first, five UWFBGs (S1-S5) with decreasing grating length of $L = 2.00$, 1.50, 1.00, 0.50, and 0.25 mm, respectively, and the same grating pitch of $\Lambda = 1.07$ μm (i.e. grating order of $K = 2$), were fabricated by using femtosecond laser with the same pulse energy of $E = 21.0$ nJ.

　The reflection spectra of UWFBGs S1-S5 were measured by using OFDR and shown in Fig. 3(a). The evolutions of peak reflectivity and bandwidth with the grating length L of the fabricated UWFBGs were extracted from Fig. 3(a) and exhibited in Fig. 3(b). It is obvious the peak reflectivity decreases and the bandwidth increases as the grating length L decreases. Moreover, in the case of UWFBG S5 with a very short grating length of 0.25 mm, a low peak

reflectivity of -44.95 dB could be obtained. However, the S5 has a large bandwidth of 2.80 nm, which is detrimental to wavelength demodulation. In the case of UWFBG S4 with a grating length of 0.50 mm, a low peak reflectivity of -39.09 dB could be obtained, but the S4 still has a large bandwidth of 1.43 nm. Furthermore, in the case of UWFBG S3 with a normal grating length of 1 mm, a bandwidth of 0.71 nm is obtained and the grating peak reflectivity is -33.06 dB. Moreover, repeated temperature measurement results show that the fabricated UWFBG with such a bandwidth of 0.71 nm has a temperature accuracy of ~0.06 °C. Therefore, we could use this grating length (i.e. $L = 1$ mm) for fabricating the subsequent UWFBGs and further reduce the peak reflectivity by increasing the grating order K and using appropriate pulse energy E.
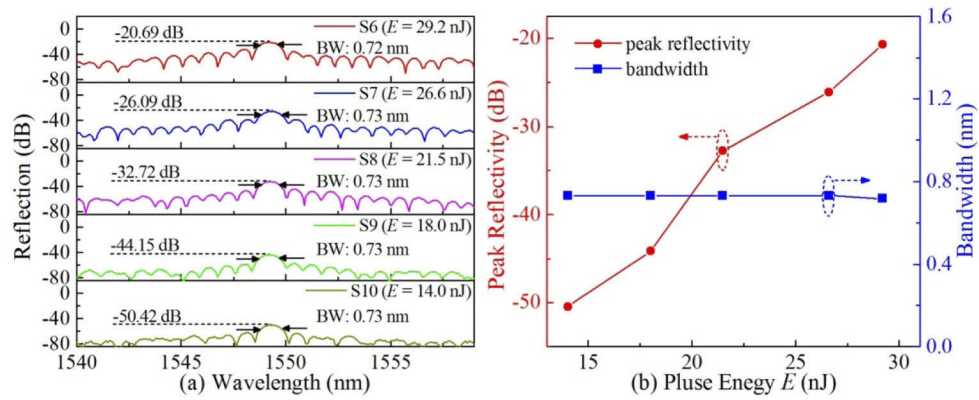

Fig. 3. Five fabricated UWFBGs S1-S5 with decreasing grating length L: (a) reflection spectra of UWFBGs S1-S5, and (b) the evolutions of peak reflectivity and bandwidths with the grating length L of the fabricated UWFBGs.

3.3. Influence of single-pulse energy on UWFBG

Subsequently, five more UWFBGs (S6-S10) with the same grating length of $L = 1$ mm and the same grating pitch of $\Lambda = 1.07$ μm (i.e. grating order of $K = 2$) were fabricated by using decreasing pulse energy E of 29.2, 26.6, 21.5, 18.0, and 14.0 nJ, respectively. The measured reflection spectra of UWFBGs S6-S10 are exhibited in Fig. 4(a), and the evolutions of peak reflectivity and bandwidths with pulse energy E are shown in Fig. 4(b). It could be seen that the peak reflectivity decreases as the pulse energy E decreases, whereas the bandwidth hardly changes. Note that the evolution of bandwidth with index modulation depth in the fabricated UWFBGs is different from that in strong FBGs, in which larger index modulation depth leads to a larger grating bandwidth. Moreover, in case a pulse energy E lower than 18.0 nJ is used, the peak reflectivity of UWFBG (i.e., S9 and S10) will be lower than -40 dB.

Furthermore, we investigated the long-term thermal stability of two UWFBGs S6 and S10 fabricated by using different femtosecond laser pulse energy of 29.2 and 14.8 nJ, respectively. The two UWFBGs S6 and S10 were annealed at a high temperature of 1000 °C for more than 35 hours. The reflection spectra of the samples were recorded by OFDR every 30 minutes. As shown in Fig. 5, the starting Bragg wavelength of S6 and S10 in the annealing experiment at 1000 °C is ~1563 nm. The Bragg wavelength of S6 and S10 exhibits a 'red' shift during the first 18.5 h, and tends to be stable after annealing for 18.5 h. This may result from the relaxation of internal stress in the UWFBG at the beginning of annealing process and subsequent formation of an extremely stable grating structure after a long-term annealing process. In addition, after annealing at 1000 °C for 18.5 hours, sample S6 exhibits a slow wavelength shift at the rate of 0.002 nm/h, which is slower than that in sample S10 (i.e. 0.005 nm/h). It means the UWFBG

Fig. 4. Five fabricated UWFBGs S6-S10 by using femtosecond laser with decreasing pulse energy E: (a) reflection spectra of UWFBGs S6-S10, and (b) the evolutions of peak reflectivity and bandwidth with the pulse energy E used for fabricating UWFBGs.

fabricated by using higher femtosecond laser pulse energy will have better high-temperature thermal stability. Moreover, after annealing at 1000 °C for 18.5 hours, the peak reflectivity of S6 and S10 change slightly and no gratings have been erased. Hence, the femtosecond laser with higher pulse energy of $E = 29.2$ nJ was used for fabricating subsequent UWFBGs with excellent long-term thermal stability at a very high temperature of 1000 °C.
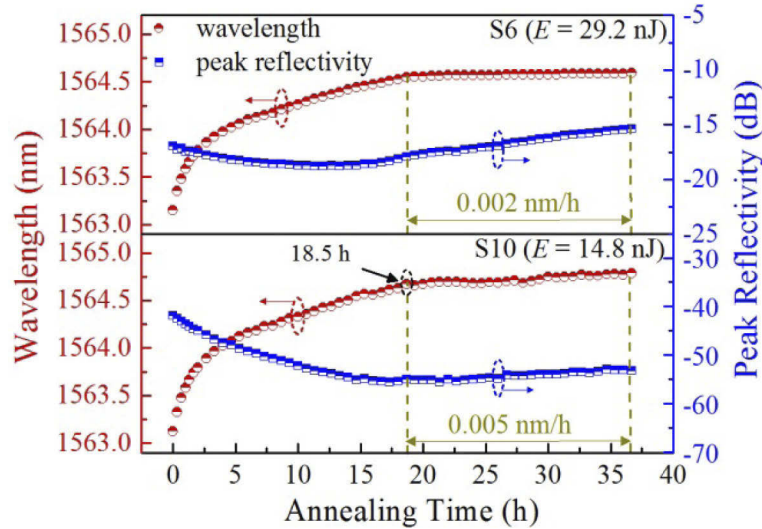

Fig. 5. Long-term high-temperature thermal stability of two UWFBGs S6 and S10 fabricated with different femtosecond laser pulse energies, showing the evolutions of Bragg wavelength and peak reflectivity when annealing at a high temperature of 1000 °C.

3.4. Influence of grating order on UWFBG

Additionally, five more UWFBGs (S11-S15) with increasing grating order of $K = 2, 16, 40, 80,$ and 120 (grating pitch $\Lambda = 1.07, 8.56, 21.40, 42.8,$ and 64.20 µm, respectively), and the same grating length of $L = 1$ mm, were fabricated by using the same laser pulse energy of $E = 29.2$ nJ. As shown in Fig. 6, the peak reflectivity of UWFBG decreases as the grating order K increases,

whereas the bandwidth hardly changes. A high-order UWFBG with $K = 120$ (i.e. S15) exhibits a low peak reflectivity of -44.87 dB and a bandwidth of 0.69 nm. As the grating order K increases, the spacing between two laser-induced points increases but the feature size of laser-induced point remains unchanged, and hence results in a decrease in the localized effective refractive index modulation $\Delta n(x, y)$ and a decrease in the reflectivity through Eqs. (2) and (3). Moreover, it should be noted that as the grating order K increases, the wavelength spacing between adjacent order peaks decreases, i.e. multiple Bragg resonance peaks emerge in the reflection spectra, as shown in Fig. 6(a).
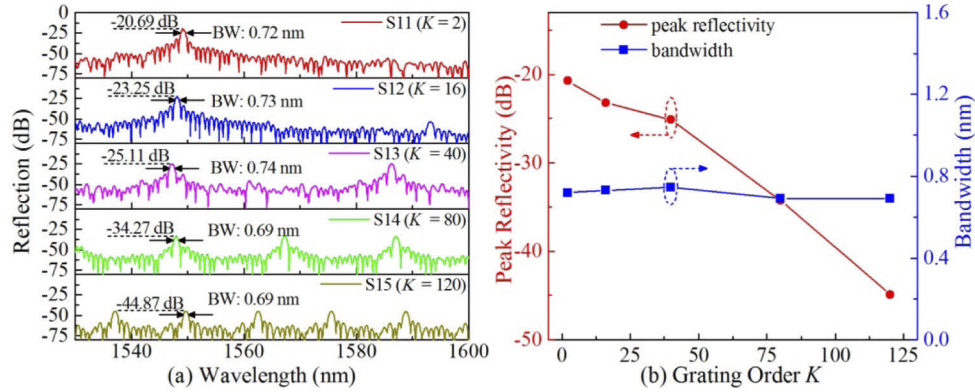
Fig. 6. Five fabricated UWFBGs S11-S15 with increasing grating order K: (a) reflection spectra of UWFBGs S11-S15, and (b) the evolutions of peak reflectivity and bandwidths with the grating order K of the fabricated UWFBGs.

4. Distributed high-temperature sensing based on the fabricated UWFBG array and OFDR

4.1. Fabrication of UWFBG array by using femtosecond laser PbP technology

After optimizing the fabrication parameters, we successfully fabricated UWFBGs with a low peak reflectivity of ∼ -45 dB (i.e. a peak reflectivity of ∼ 0.0032%) by using the femtosecond laser PbP technology with a laser pulse energy of $E = 29.2$ nJ, a grating length of $L = 1$ mm, and a grating order of $K = 120$ (a grating pitch of $\Lambda = 64.2$ μm). Moreover, a UWFBG array consisting of 200 identical UWFBGs was automatically fabricated in a 2 meters-long SMF by using these fabrication parameters. Note that no pre-removal of the fiber coating was required in this process since the UWFBGs could be inscribed by focusing the femtosecond laser beam through the fiber coating, and it takes ∼1 h to fabricate such a UWFBG array. Moreover, the fabricated UWFBG array was interrogated by using the OFDR together with a 12.1 m-long lead-in SMF, and the results are shown in Fig. 7. The demodulation results of the fabricated UWFBG array are shown in frequency domain in Figs. 7(a) and 7(b), in which 200 UWFBGs with a grating length L of 1 mm, a spacing of 10 mm, and a total array length of ∼ 2 m could be observed. The non-uniformity in the reflection amplitude of these UWFBGs could be seen clearly in Fig. 7(a). This may result from the fluctuation in femtosecond laser pulse energies, the inhomogeneity in the fiber core, and/or the positioning errors in image recognition process. In addition, the reflection spectrum of the 90th UWFBG is shown in Fig. 7(c), exhibiting a 120th-order Bragg wavelength of 1548.8 nm and a peak reflection of -44.97 dB. Note that the 119th-order Bragg wavelength of 1561.7 nm and the 121th-order Bragg wavelength of 1536.1 nm could also be observed in the spectrum. The spacing between adjacent Bragg wavelengths is ∼ 12.9 nm, which is consistent with the result calculated from equation $m\lambda = 2n\Lambda$. Furthermore, the accumulated transmission

loss was recorded for every 50 UWFBGs during the fabrication process and is demonstrated in Fig. 7(d). As the number of fabricated UWFBGs in the array increases, the transmission loss also increases, exhibiting a transmission loss of 0.01047 dB per UWFBG. This means the largest number of multiplexed UWFBGs in the array can reach more than 2000. Moreover, it should be noted that the insertion loss of such a UWFBG is significantly lower than that in a conventional femtosecond laser-induced type II FBG (typically ∼ 1 dB) [29,30,33,34]. This may partially result from the lower pulse energy used for fabricating such a UWFBG, and partially result from the much higher grating order in the UWFBG, which means there are fewer modulation points in the UWFBG, leading to lower scattering loss in this type of gratings.
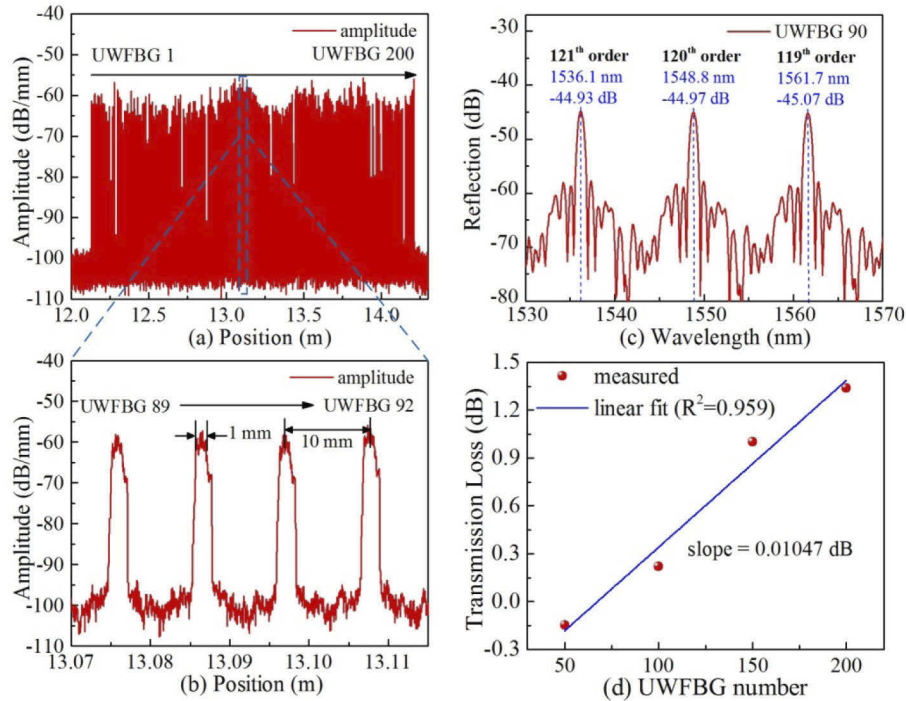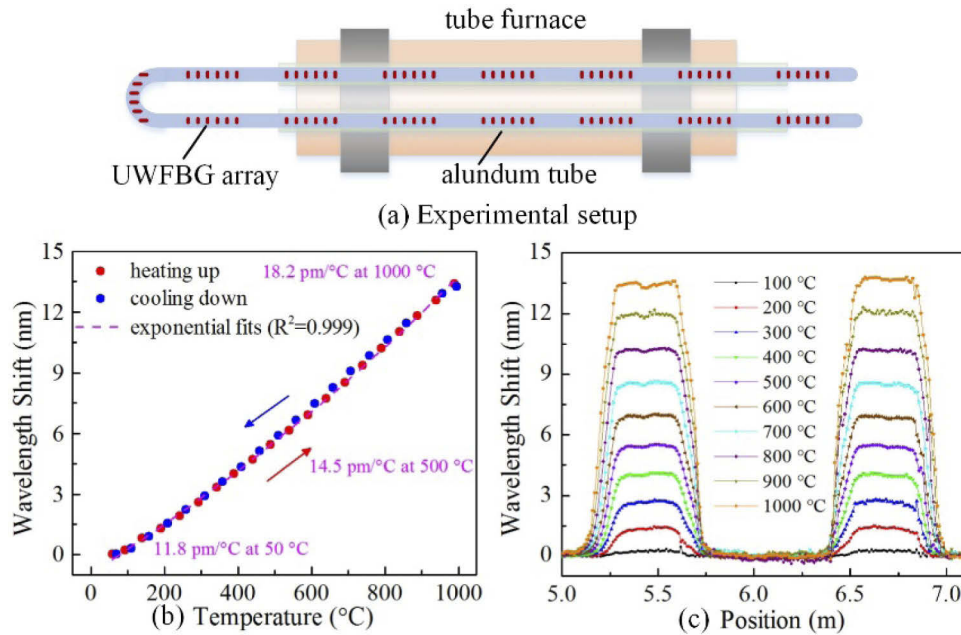

Fig. 7. (a) Demodulation result of the fabricated UWFBG array in frequency domain, showing the position of each UWFBG in the array; (b) zoom-in of (a) at a specific region at 13.070 - 13.115 m, showing the reflection from the 89th to the 92th UWFBG in frequency domain; (c) the reflection spectrum of the 90th UWFBG in the array; (d) accumulated transmission loss as a function of increasing number of UWFBGs.

4.2. Distributed high-temperature sensing

Furthermore, a distributed high-temperature sensing experiment was carried out by using the fabricated UWFBG array and the OFDR-based wavelength demodulation. The UWFBG array has been annealed at a high temperature of 1000 °C for 18.5 hours. As shown in Fig. 8(a), the UWFBG array under test was placed in a tube furnace (Carbolite 301) by threading the fiber back and forth through an alundum tube. Hence, two sections of UWFBG array with each length of ∼ 40 cm were placed in the heated region of tube furnace, and the rest section was placed in the unheated region. Moreover, a lead-in SMF with a length of ∼ 5 m was used for interrogating the UWFBG array. A thermocouple was placed in the center of tube furnace to record the temperature, which was varied between 50 and 1000 °C and maintained for 30 min at each measurement point. The 120th-order Bragg wavelength (as shown in Fig. 7(c)) of each

UWFBG was recorded at each measurement point, and the corresponding wavelength shifts were calculated. As shown in Fig. 8(b), the wavelength shift of the 30th UWFBG exhibits a 'red' shift with an increasing temperature and a 'blue' shift with a decreasing temperature. Then, the measured results are well fitted by exponential curves, in which excellent thermal repeatability is exhibited with an increasing temperature sensitivity at elevated temperatures, i.e. 11.8 pm/°C at a low temperature of 50 °C, 14.5 pm/°C at a medium temperature of 500 °C, and 18.2 pm/°C at a high temperature of 1000 °C. This results from the increasing thermal-optic coefficient of silica at high temperatures. As shown in Fig. 8(c), the temperature field distributions in the tube furnace under different thermal conditions can be reconstructed from the wavelength shift of each UWFBG in the array placed at different positions in the furnace. Consequently, the fabricated UWFBG array could be used for distributed high-temperature sensing of up to 1000 °C.

Fig. 8. Distributed high-temperature sensing based on the fabricated UWFBG array and OFDR-based wavelength demodulation: (a) schematic of the UWFBG array placed in a tube furnace; (b) wavelength shift of the 30th UWFBG in the array as functions of temperature increasing and decreasing between 50 and 1000 °C, and (c) measured wavelength shift of each UWFBG in the array at different positions, illustrating the temperature field distributions under different thermal conditions. (Note that the temperatures shown in this figure were recorded by a thermocouple placed in the furnace center)

5. Conclusion

We have demonstrated a new method for automatically fabricating high-temperature-resistant UWFBG arrays by using a femtosecond laser PbP technology. Effects of pulse energy, grating length, and grating order used for fabricating UWFBGs were studied, and UWFBGs with a low peak reflectivity of ∼ - 45 dB (i.e. ∼ 0.0032%) were successfully fabricated by using appropriate fabrication parameters, including a grating length of 1 mm, pulse energy of 29.2 nJ, and a grating order of 120. Moreover, a long-term thermal stability of the fabricated UWFBGs was studied. The UWFBGs could withstand a high temperature of 1000 °C for long time and have an excellent thermal repeatability with a sensitivity of 18.2 pm/°C at 1000 °C. Subsequently, a UWFBG array

consisting of 200 identical UWFBGs was fabricated along a 2 m conventional SMF with an interval of 10 mm and was used to realize distributed high-temperature sensing up to 1000 °C based on OFDR demodulation. As a result, the proposed femtosecond laser-inscribed UWFBG array can be developed for distributed high-temperature sensing in harsh environments, such as hypersonic vehicles, aero engines, nuclear plants, power stations, and smelting furnaces.

Disclosures. The authors declare no conflicts of interest.

Data availability. Data underlying the results presented in this paper are not publicly available at this time but may be obtained from the authors upon reasonable request.

References

1. P. Lu, N. Lalam, M. Badar, B. Liu, B. T. Chorpening, M. P. Buric, and P. R. Ohodnicki, "Distributed optical fiber sensing: review and perspective," Appl. Phys. Rev. **6**, 041302 (2019).
2. M. A. Soto, T. Nannipieri, A. Signorini, A. Lazzeri, F. Baronti, R. Roncella, G. Bolognini, and F. D. Pasquale, "Raman-based distributed temperature sensor with 1 m spatial resolution over 26 km SMF using low-repetition-rate cyclic pulse coding," Opt. Lett. **36**(13), 2557–2559 (2011).
3. Y. P. Liu, L. Ma, C. Yang, W. J. Tong, and Z. Y. He, "Long-range Raman distributed temperature sensor with high spatial and temperature resolution using graded-index few-mode fiber," Opt. Express **26**(16), 20562–20571 (2018).
4. F. Wang, C. H. Zhu, C. Q. Cao, and X. P. Zhang, "Enhancing the performance of BOTDR based on the combination of FFT technique and complementary coding," Opt. Express **25**(4), 3504–3513 (2017).
5. X. Bao, D. J. Webb, and D. A. Jackson, "32-km distributed temperature sensor based on Brillouin loss in an optical fiber," Opt. Lett. **18**(18), 1561–1563 (1993).
6. J. Song, W. H. Li, P. Lu, Y. P. Xu, L. Chen, and X. Y. Bao, "Long-range high spatial resolution distributed temperature and strain sensing based on optical frequency-domain reflectometry," IEEE Photonics J. **6**(3), 1–8 (2014).
7. M. M. Luo, J. F. Liu, C. J. Tang, X. F. Wang, T. Lan, and B. X. Kan, "0.5 mm spatial resolution distributed fiber temperature and strain sensor with position-deviation compensation based on OFDR," Opt. Express **27**(24), 35823–35829 (2019).
8. A. K. Sang, M. E. Froggatt, D. K. Gifford, and B. D. Dickerson, "One centimeter spatial resolution temperature measurements from 25 to 850 °C using Rayleigh scatter in gold coated fiber," CLEO JTuA, JTuA77 (2007).
9. P. B. Xu, D. X. Ba, W. M. He, H. P. Hu, and Y. K. Dong, "Distributed Brillouin optical fiber temperature and strain sensing at a high temperature up to 1000 °C by using an annealed gold-coated fiber," Opt. Express **26**(23), 29724–29734 (2018).
10. P. B. Xu, Y. K. Dong, D. W. Zhou, C. Fu, J. W. Zhang, H. Y. Zhang, Z. W. Lu, L. Chen, and X. Y. Bao, "1200°C high-temperature distributed optical fiber sensing using Brillouin optical time domain analysis," Appl. Opt. **55**(21), 5471–5478 (2016).
11. B. Liu, Z. H. Yu, C. Hill, Y. J. Cheng, D. Homa, G. Pickrell, and A. B. Wang, "Sapphire-fiber-based distributed high-temperature sensing system," Opt. Lett. **41**(18), 4405–4408 (2016).
12. B. Liu, M. P. Buric, B. T. Chorpening, Z. H. Yu, D. S. Homa, G. R. Pickrell, and A. B. Wang, "Design and implementation of distributed ultra-High temperature sensing system with a single crystal fiber," J. Lightwave Technol. **36**(23), 5511–5520 (2018).
13. X. Gui, Z. Y. Li, F. Wang, Y. M. Wang, C. J. Wang, S. Y. Zeng, and H. H. Yu, "Distributed sensing technology of high-spatial resolution based on dense ultra-short FBG array with large multiplexing capacity," Opt. Express **25**(23), 28112–28122 (2017).
14. C. J. Wang, Z. Y. Li, X. Gui, X. L. Fu, F. Wang, H. H. Wang, J. Q. Wang, and X. Y. Bao, "Micro-cavity array with high accuracy for fully distributed optical fiber sensing," J. Lightwave Technol. **37**(3), 927–932 (2019).
15. Y. M. Wang, J. M. Gong, D. Y. Wang, B. Dong, W. H. Bi, and A. B. Wang, "A quasi-distributed sensing network with time-division-multiplexed fiber Bragg gratings," IEEE Photonics Technol. Lett. **23**(2), 70–72 (2011).
16. C. L. Li, J. G. Tang, C. Cheng, L. B. Cai, and M. H. Yang, "FBG arrays for quasi-distributed sensing: a review," Photonic Sens **11**(1), 91–108 (2021).
17. M. H. Yang, W. Bai, H. Y. Guo, H. Q. Wen, H. H. Yu, and D. S. Jiang, "Huge capacity fiber-optic sensing network based on ultra-weak draw tower gratings," Photonic Sens **6**(1), 26–41 (2016).
18. Y. M. Wang, J. M. Gong, B. Dong, D. Y. Wang, T. J. Shillig, and A. B. Wang, "A large serial time-division multiplexed fiber Bragg grating sensor network," J. Lightwave Technol. **30**(17), 2751–2756 (2012).
19. L. Dong, J. L. Archambault, L. Reekie, S. P. J. Russell, and D. N. Payne, "Single pulse Bragg gratings written during fibre drawing," Electron. Lett. **29**(17), 1577–1578 (1993).
20. E. Lindner, J. Mrbitz, C. Chojetzki, M. Becker, S. Brckner, K. Schuster, M. Rothhardt, and H. Bartelt, "Draw tower fiber Bragg gratings and their use in sensing technology," Proc. SPIE **8028**, 80280C (2011).
21. E. Lindner, J. Canning, C. Chojetzki, S. Bruckner, M. Becker, M. Rothhardt, and H. Bartelt, "Post-hydrogen-loaded draw tower fiber Bragg gratings and their thermal regeneration," Appl. Opt. **50**(17), 2519–2522 (2011).

22. H. Y. Guo, J. G. Tang, X. F. Li, Y. Zheng, H. Yu, and H. H. Yu, "On-line writing identical and weak fiber Bragg grating arrays," Chin. Opt. Lett. **11**(3), 030602 (2013).
23. H. Y. Guo, F. Liu, Y. Q. Yuan, H. H. Yu, and M. H. Yang, "Ultra-weak FBG and its refractive index distribution in the drawing optical fiber," Opt. Express **23**(4), 4829–4838 (2015).
24. S. Liu, G. H. He, Z. Zheng, L. Y. Ding, A. Zhou, H. Y. Guo, C. M. Zhou, and D. S. Jiang, "Importance of internal tensile stress in forming low-loss fiber draw-tower gratings," J. Lightwave Technol. **38**(7), 1900–1904 (2020).
25. X. Gui, Z. Y. Li, X. L. Fu, C. J. Wang, H. H. Wang, F. Wang, and X. Y. Bao, "Large-scale multiplexing of a FBG array with randomly varied characteristic parameters for distributed sensing," Opt. Lett. **43**(21), 5259–5262 (2018).
26. S. Liu, L. Y. Ding, H. Y. Guo, A. Zhou, C. M. Zhou, L. Qian, H. H. Yu, and D. S. Jiang, "Thermal stability of drawing-tower grating written in a single mode fiber," J. Lightwave Technol. **37**(13), 3073–3077 (2019).
27. J. Canning, "Fibre gratings and devices for sensors and lasers," Laser & Photon. Rev. **2**(4), 275–289 (2008).
28. K. Chah, K. Yüksel, D. Kinet, N. S. Yazd, P. Mégret, and C. Caucheteur, "Fiber Bragg grating regeneration at 450° C for improved high temperature sensing," Opt. Lett. **44**(16), 4036–4039 (2019).
29. H. Chikh-Bled, K. Chah, Á. González-Vila, B. Lasri, and C. Caucheteur, "Behavior of femtosecond laser-induced eccentric fiber Bragg gratings at very high temperatures," Opt. Lett. **41**(17), 4048–4051 (2016).
30. J. He, B. J. Xu, X. Z. Xu, C. R. Liao, and Y. P. Wang, "Review of femtosecond-laser-inscribed fiber Bragg gratings: fabrication technologies and sensing applications," Photonic Sens **11**(2), 203–226 (2021).
31. A. Martinez, I. Y. Khrushchev, and I. Bennion, "Thermal properties of fibre Bragg gratings inscribed point-by-point by infrared femtosecond laser," Electron. Lett. **41**(4), 176 (2005).
32. J. He, Y. P. Wang, C. R. Liao, C. Wang, S. Liu, K. M. Yang, Y. Wang, X. C. Yuan, G. P. Wang, and W. J. Zhang, "Negative-index gratings formed by femtosecond laser overexposure and thermal regeneration," Sci. Rep. **6**(1), 23379 (2016).
33. C. W. Smelser, S. J. Mihailov, and D. Grobnic, "Formation of type I-IR and type II-IR gratings with an ultrafast IR laser and a phase mask," Opt. Express **13**(14), 5377–5386 (2005).
34. C. R. Liao, Y. H. Li, D. N. Wang, T. Sun, and K. T. V. Grattan, "Morphology and thermal stability of fiber Bragg gratings for sensor applications written in H_2-free and H_2-loaded fibers by femtosecond laser," IEEE Sensors J. **10**(11), 1675–1681 (2010).
35. S. C. Warren-Smith, L. V. Nguyen, C. Lang, H. E. Heidepriem, and T. M. Monro, "Temperature sensing up to 1300°C using suspended-core microstructured optical fibers," Opt. Express **24**(4), 3714–3719 (2016).
36. X. Z. Xu, J. He, C. R. Liao, K. M. Yang, K. K. Guo, C. Li, Y. F. Zhang, Z. B. Ouyang, and Y. P. Wang, "Sapphire fiber Bragg gratings inscribed with a femtosecond laser line-by-line scanning technique," Opt. Lett. **43**(19), 4562–4565 (2018).
37. B. J. Soller, D. K. Gifford, M. S. Wolfe, and M. E. Froggatt, "High resolution optical frequency domain reflectometry for characterization of components and assemblies," Opt. Express **13**(2), 666–674 (2005).
38. T. Erdogan, "Fiber grating spectra," J. Lightwave Technol. **15**(8), 1277–1294 (1997).